Synthesis of Mn doped nanostructured zinc oxide thin films for H_2 gas sensing

M. F. Allawai[a], M. S. Sada[b], A. M. Jabbar[c], K. N. Hussein[d], N. F. Habubi[e], S. S. Chiad[f], M. Jadan[g, h,*]
[a]*Department of medical physics, College of Applied Science, University of Fallujah, Iraq*
[b]*Department of Physics, College of Education, University of Masan, Iraq*
[c]*Department of Physics, College of Science, Mustansiriyah University, Iraq*
[d]*Department of Radiology, Al-Manara College for Medical Science, Iraq*
[e]*Department of Radiation and Sonar Technologies, Al-Nukhba University College, Iraq*
[f]*Department of Physics, College of Education, Mustansiriyah University, Iraq*
[g]*Department of Physics, College of Science, Imam Abdulrahman Bin Faisal University, P.O. Box 1982, 31441 Dammam, Saudi Arabia*
[h]*Basic and Applied Scientific Research Center, Imam Abdulrahman Bin Faisal University, P.O. Box 1982, 31441 Dammam, Saudi Arabia*

Thin films of zinc oxide and (ZnO:Mn) with 1% and 3% concentrations were created at 400 °C by spray pyrolysis. According to X-ray diffraction (XRD) investigation, ZnO films are polycrystalline and have a cubic structure with a distinct peak in one direction (101). The grain size increases as manganese content rise, from 12.66 nm to 14.66 nm. While the strain (ε) for ZnO reduced after manganese doping, it decreased from 27.36 to 23.63. Surface topography and nanostructure study reveal that as the manganese (Mn) content of ZnO films increased, cluster grain size, average roughness, and root mean square roughness (Rrms) all significantly reduced. SEM images show substantial morphological changes from flat islands to spherical nano-grains post-manganese via Mn content. The average transmittance was >70% in the visible area for Undoped ZnO and 1, 3% Manganese doping optical transmittance demonstrates exceptional optical transparency. When doping levels are increased by 1% or 3%, the absorption coefficient rises. The optical band gap widens in ZnO: Mn film for allowed direct transition has been decreased from (3.32 to 3.21) eV. Results illustrate that the films' refractive index and extinction coefficient decreases with increasing Mn Doped. Hydrogen gas decreases resistance in ZnO films, suggesting p-type behavior. Doping with 3% Mn increases resistance. Decreased sensitivity with higher Mn content after hydrogen gas exposure indicates increased electrical resistance in the film.

(Received February 26, 2024; Accepted May 27, 2024)

Keywords: ZnO, Mn, XRD, Topography, Band gap

1. Introduction

Zinc oxide (ZnO) possesses distinctive characteristics, including being an n-type semiconductor, exhibiting high transparency, and demonstrating elevated electron mobility and thermal conductivity. Zinc oxide has many applications due to its excellent optical, photoelectric, and piezoelectric properties. Thus, this approach is ideal for realizing optical devices, including LED , and solar cells,. In the applications above, zinc oxide (ZnO) with a hexagonal wurzite structure has recently shown potential as an ITO alternative [1-4]. It is particularly interested in wide bandgap semiconductors due to the growing commercial need for short-wavelength LED [5-7]. ZnO-nanostructured films are a great option because of their wide bandgap (3.37 eV) and high exciton binding energy of 60 mV [8-11]. ZnO is grown using a variety of techniques, such as dip

* Corresponding author: muhannadjadan99@gmail.com
https://doi.org/10.15251/DJNB.2024.192.793

coating [12], chemical vapor deposition [13], hydrothermal growth [14], thermal vacuum evaporation [15], RF sputtering [16], electrodeposition [17], atomic layer deposition [18] and SPM [19], Spray pyrolysis is one of these techniques suitable for broad-area thin film production and simple doping [20]. This paper reports the experimental findings of physical attributes discovered using various characterization methods. The thin films under study were applied to a glass substrate using spray pyrolysis, which can produce large-area films with good optical properties and crystalline at a low cost. The temperature and deposition time are crucial because this is a chemical procedure. This work aims to show Mn's effect on the physical characterization and gas sensing.

2. Experimental

The current study used CSP to manufacture Mn-doped ZnO film on a glass slide substrate. Thin films of ZnO were produced using this technique. 0.1 M of $ZnCl_2$ dissolved in the 1:1 mixture of deionized water and ethanol was used to manufacture ZnO thin films. The doping substance was manganese trichloride ($MnCl_3$), which was dissolved in deionized water, and a few drops of hydrochloric acid were added so the solution would be transparent. The following are the requirements for preparation: Base temperature was 400 ^oC, there was a distance of 28 cm between spout and base, and the spraying period was 8 s , but it was prolonged by 65 seconds to prevent cooling, the spray rate was 5 ml/min, and N_2 was used as the transporter gas. The thickness was determined using the gravimetric method of 340 ± 20 nm. The thin film ZnO generated was established by XRD analysis, and AFM was used to evaluate the films' structure and morphology. SEM images were acquired utilizing a multi-function scanning electron microscope model ALS 2300 Angstrom. Transmittance is estimated using a UV-Vis NIR. A gas sensor was developed using undoped ZnO and Mn-doped ZnO thin films featuring aluminum electrodes. The gas sensitivity was assessed based on the percentage change in resistance within a cylindrical chamber (radius: 8.5 cm, height: 17 cm).

3. Results and discussions

Figure (1) presents the XRD patterns of the ZnO thin film synthesized through a simple chemical method before annealing. The peaks at angles of 31.73°, 36.24°, 47.42°, and 62.65° correspond to the (100), (101), (102), and (103) planes, respectively [21, 22]. These peaks indicate a polycrystalline nature and a preferred orientation along the (101) direction, as confirmed by the ICDD card number (36.1451), revealing a crystalline structure with a specific orientation[10]. The grain size (D) was calculated using Scherrer's Eq. (1) [23, 24]:

$$D = \frac{0.9\,\lambda}{\beta cos\theta} \tag{1}$$

where λ is the X-rays' wavelength, β and θ are FWHM and the Bragg angle of (101) peak, respectively. The results presented in Table (1) indicate an increase in *D* from 12.66 to 14.66 nm with the addition of ZnO: 3% Mn. This suggests that the manganese content plays a crucial role in adjusting the crystal sizes [25, 26].

Evaluation is also done on other structural metrics, including dislocation density (δ) from Eq. 2 [27, 28].

$$\delta = \frac{1}{D^2} \tag{2}$$

The calculation of the strain (ε) is calculated using the following equation [29, 30]:

$$\varepsilon = \frac{\beta cos\theta}{4} \tag{3}$$

Table (1) presents the data, indicating a reduction in strain with an increase in manganese content. The improvement in crystalline quality is attributed to the regular atom arrangements in the crystal lattice [31, 32]. These findings suggest a fundamental impact of manganese concentration on crystallite size, decreasing from 12.66 to 14.66. Fig. (2) depicts the structural parameters (S¬para) as functions of manganese concentration.

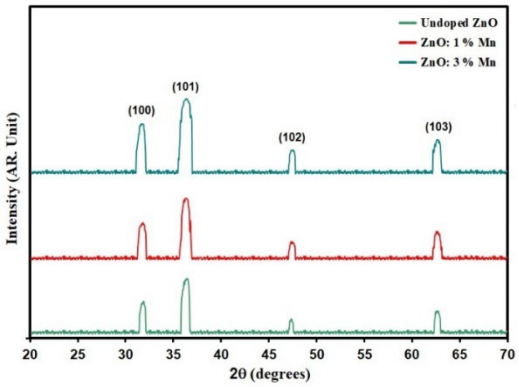

Fig. 1. XRD patterns.

Table 1. D, optical bandgap and S_{para} of prepared films.

Specimen	2 □ (°)	(hkl) Plane	FWHM (°)	E_g (eV)	*D* (nm)	δ (× 10^{14}) (lines/m^2)	E (×10^{-4})
Undoped ZnO	36.24	101	0.66	3.32	12.66	62.33	27.36
ZnO: 1% Mn	36.21	101	0.62	3.26	13.48	54.97	25.70
ZnO: 3% Mn	36.17	101	0.57	3.21	14.66	46.47	23.63

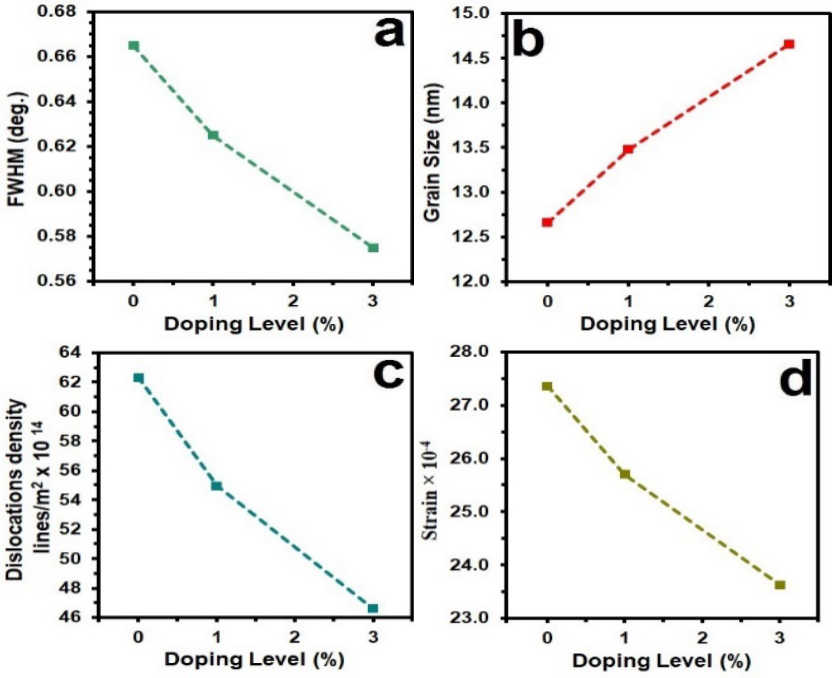

Fig. 2. S_{Para} of the grown films.

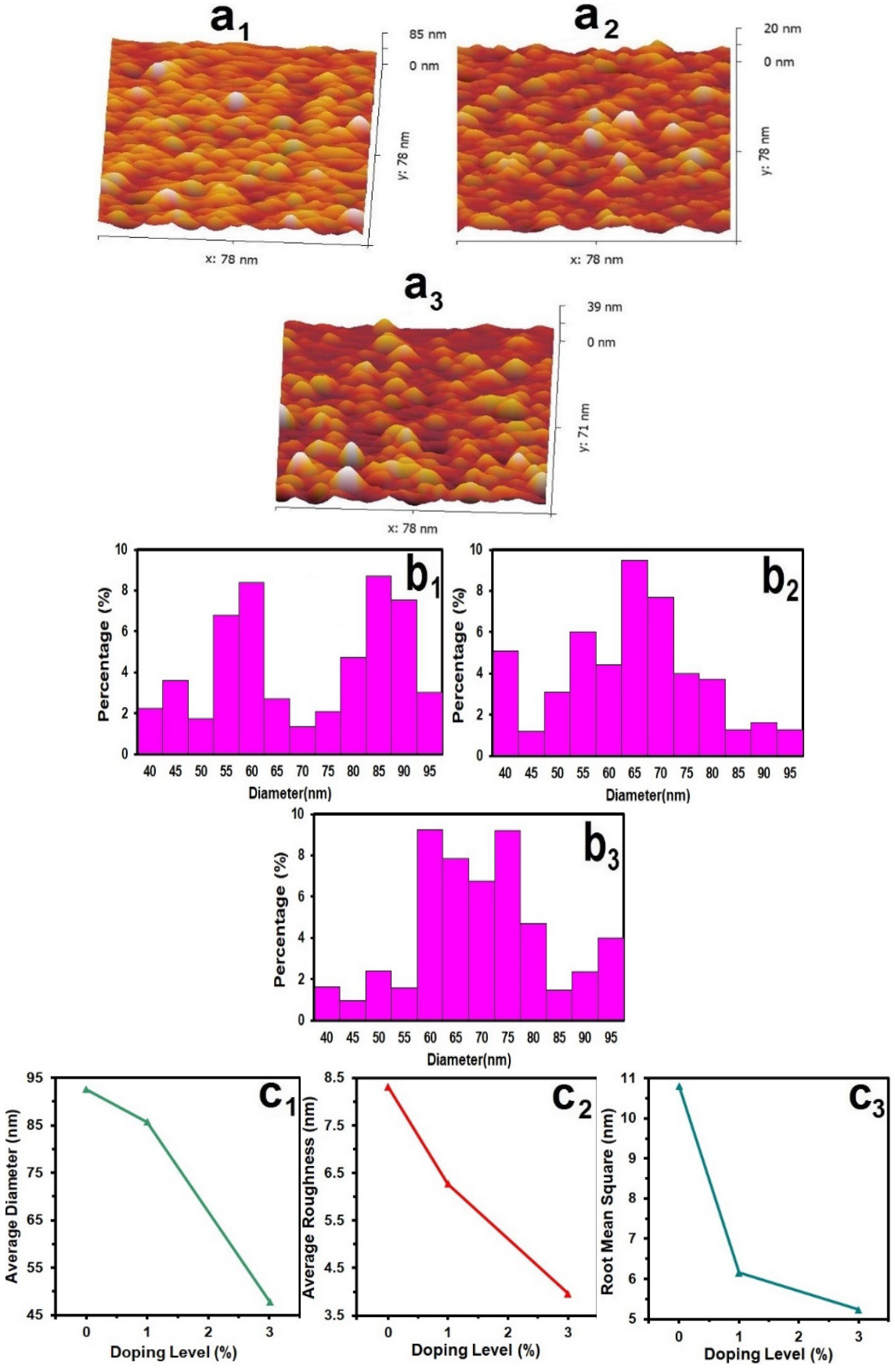

Fig. 3. AFM informations of the grown films.

The AFM image in Figure 3 reveals the three-dimensional surface morphology of zinc oxide films produced by SPM. Table 1 summarizes the films' average particle size (P_{av}), Rrms, and roughness (Ra). Average particle sizes for ZnO, ZnO:1% Mn, and ZnO:3% Mn were (92.6), (85.7), and (47.8) nm, respectively. As the doping increases, the Rrms value for as-deposited ZnO thin films decreases to 1.99 nm [33]. The Ra roughness parameters, as depicted in Figs. 3(a_3), (b_3), and (c_3), exhibit a trend with dopant concentration. Detailed AFM parameter P_{AFM} values are presented in Table 2.

Table 2. P_{AFM} of the intended films.

Samples	**P_{av} nm**	**R_a (nm)**	**R_{rms} (nm)**
Undoped ZnO	92..6	8.31	10.81
ZnO: 1% Mn	85.7	6.27	6.15
ZnO: 3% Mn	47.8	3.96	5.23

The morphological changes observed in the SEM images (Figure 4) indicate that Manganese doping in the synthesized films, consisting of undoped and manganese-doped ZnO, significantly influences the film morphology. Initially, the surface exhibits distinct, virtually flat islands [19]. However, a notable transformation occurs with an increase in manganese doping, resulting in a uniform surface coverage with spherical nano-grains. The decreasing size of these nano-grains as Manganese doping concentration increases implies a correlation between the level of manganese doping and the resulting nanostructure. This highlights the substantial impact of increased Manganese doping on shaping the film morphology [34, 35].

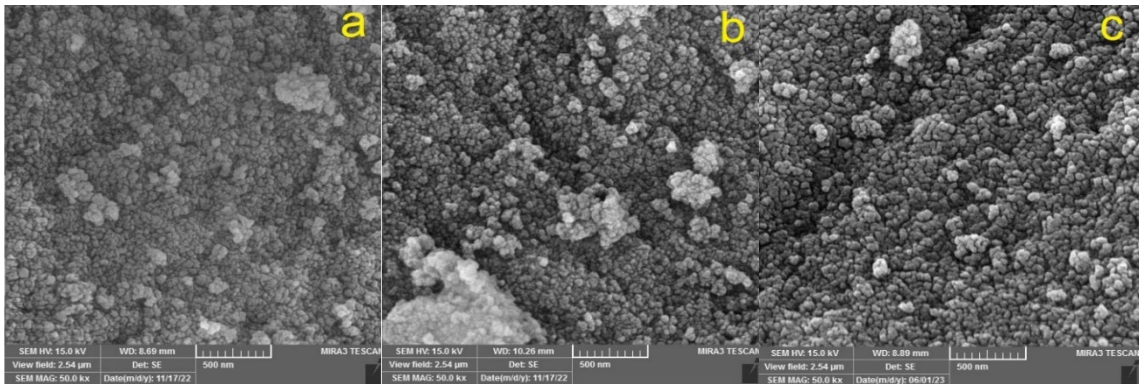

Fig. 4. SEM images (a) udoped ZnO (b) 1% doped by Mn (c) 3% doped by Mn.

The transmittance is calculated from equation 4 [36]:

$$\% = \frac{I}{I_o}\% \tag{4}$$

where (Io) is the initial light intensity and (I) is the light intensity after it passes through the sample. Fig. (5) displays the transmittance (T) spectra of ZnO film and doped films. The decrease in transmittance observed in Figure (5) with increasing manganese content indicates that the introduction of Manganese into the ZnO film impacts its optical properties. The reduction in transmittance may be attributed to the influence of Manganese on the crystal structure and optical properties of the ZnO film, leading to changes in its optical behavior [20].

The absorption coefficient (α) is determined [37, 38]:

$$\alpha = 2.303(A/T) \tag{5}$$

where t is the film thickness, The observed increase in the absorption coefficient (α) with an elevation in manganese doping, as depicted in Fig. 6, signifies a notable influence of manganese on the optical properties of the ZnO thin films [39].

The energy gap E_g is plotted following Tauc relation [40, 41]:

$$(\alpha h\nu) = A\left(h\nu - E_g\right)^{\frac{1}{2}} \tag{6}$$

where A is the constant, ν is the incoming radiation's frequency, and h is Planck's constant; Figure 7 displays the resulting graph, illustrating the energy gap values of ZnO and manganese-doped ZnO films. The energy gap for ZnO is approximately 3.32 eV, while the manganese-doped ZnO film exhibits a reduced energy gap of about 3.21 eV. This decrease in the energy gap indicates a modification in the material's electronic structure due to the incorporation of Manganese. The observed trend aligns with findings reported by other researchers [8, 42].

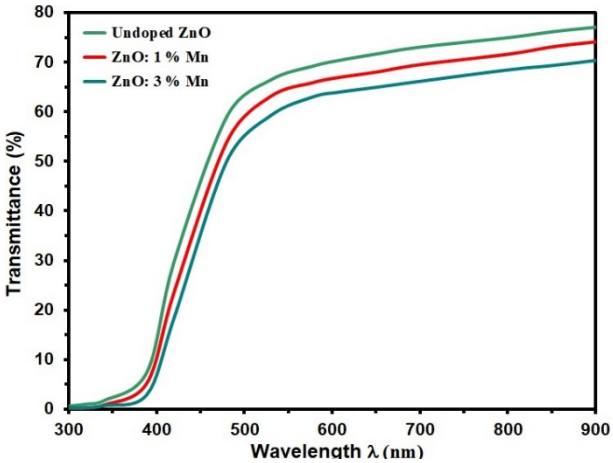

Fig. 5. Transmittance versus wavelength of the grown films.

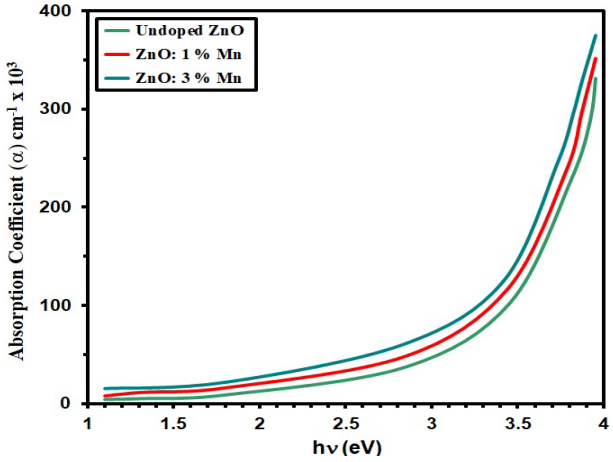

Fig. 6. Absorption coefficient versus hν for deposited films.

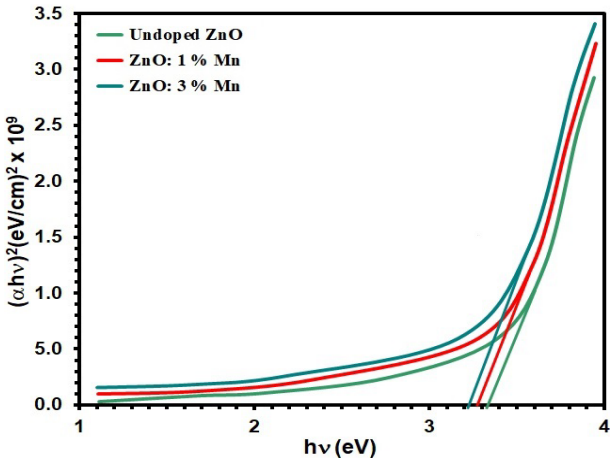

Fig. 7. $(\alpha hv)^2$ versus hv for the ZnO with different Mn doping.

The extinction coefficient (K) is meaured by Eq. 7 [43, 44]:

$$k = \frac{\alpha\lambda}{4\pi} \tag{7}$$

The observed change in the extinction coefficient (k) in Figure 8 indicates a slight reduction after magnesium doping. This reduction is linked to the wavelength of polarized light. However, it is noteworthy that k quickly regains its absorption characteristic, emphasizing the dynamic nature of the material's optical properties following Manganese doping [45].

Eq. 8 obtains the refractive index (n)[46, 47]:

$$n = \left(\frac{1+R}{1-R}\right) + \sqrt{\frac{4R}{(1-R)^2} - k^2} \tag{8}$$

where R is the reflectance, In Figure 9, the observed trend demonstrates a marginal decrease in the refractive index (n) with increasing manganese content, as plotted against wavelength (λ). This suggests that the incorporation of Manganese influences the optical properties of the material, resulting in a slight reduction in refractive index [19, 48].

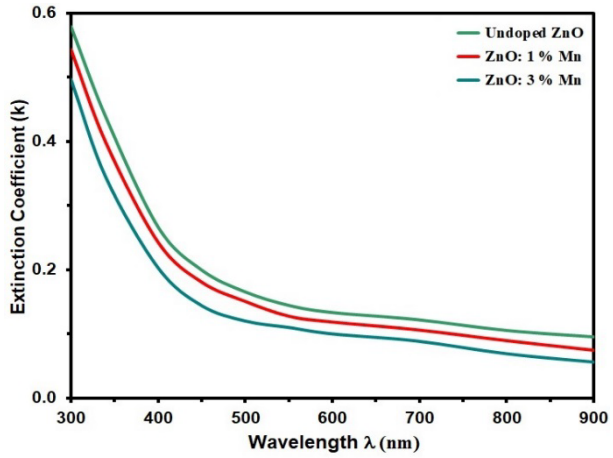

Fig. 8. k of the grown films.

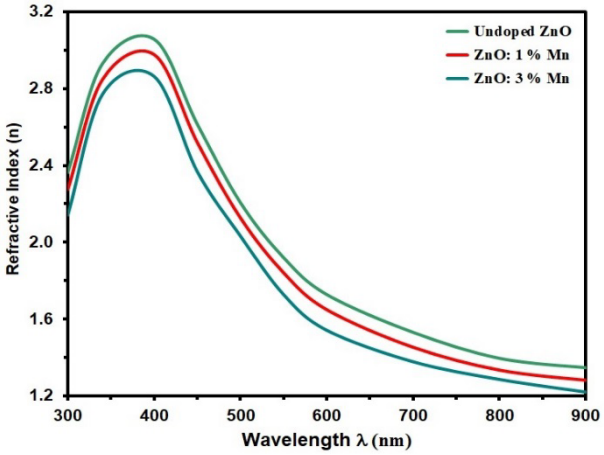

Fig. 9. n for grown films.

In Fig. (10), the resistance via response time is depicted for films with undoped ZnO and manganese-doped ZnO. The observed decrease in resistance for all samples upon introducing Hydrogen gas into the chamber indicates that ZnO behaves as a p-type semiconductor. This suggests that oxidizing gases like hydrogen molecules (H_2) (a concentration of 180 ppm.) react with the film surface, capturing electrons from the conduction band. This process increases the number of holes (majority charge carriers in p-type semiconductors) in the conduction band, reducing film resistance [49].The ZnO:Mn doping at 3% concentration also demonstrated the highest resistance, suggesting the impact of doping on the semiconductor properties of the films [17].

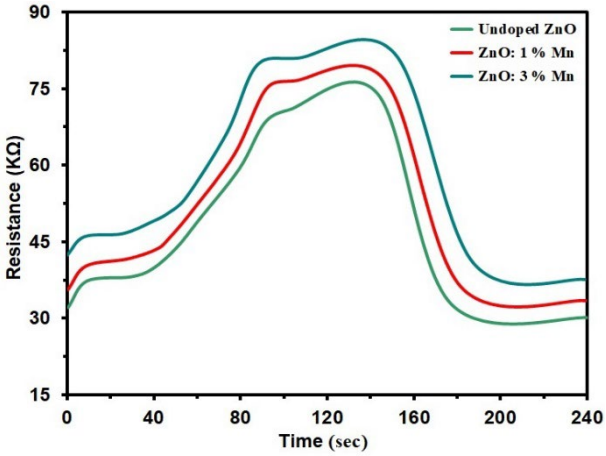

Fig. 10. Resistance as a function of operating time for Undoped and ZnO: Mn films with different dopant.

The percentage change in resistance after exposure to gas is a popular way to determine a film's sensitivity (S). This can be expressed as the ratio of the resistance in air to the steady-state value when gas is present [50]. The following formula can be used to determine the sensor's response or detection sensitivity [51, 52]:

$$\text{Sensitivity} = \frac{\Delta R}{R_g} = \left|\frac{R_g - R_a}{R_g}\right| \times 100\ \% \tag{9}$$

The decrease in sensitivity with increasing Tin content, as observed in the sensitivity plots in Figure (11) after exposure to hydrogen gas, can be attributed to the heightened electrical

resistance of the film. This increase in resistance results from the recombination process between the charge carriers of holes and electrons released from oxygen. Specifically, the reduction in sensitivity from 53.6% to 20.1% for 180 ppm, from 49.9% to 14.7% for 180 ppm, and from 46.4% to 12.2% for 90 ppm for undoped ZnO and Tin-doped ZnO, respectively, suggests that the doping concentration influences the film's response to hydrogen gas [53].

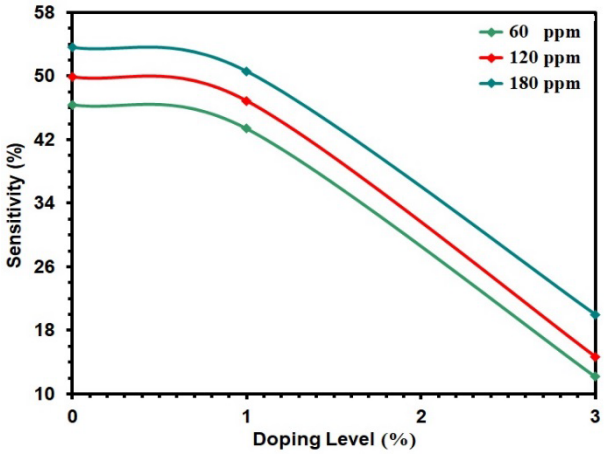

Fig. 11. Sensitivity of Undoped and ZnO: Mn films with different dopant.

4. Conclusion

We looked at spray pyrolysis-deposited thin films of zinc oxide. According to XRD findings, annealed ZnO films have a preferred orientation of 101 degrees. Microstructural parameters have been computed for prepared samples. Particle size increases as the manganese content does, from 12.66 nm to 14.66 nm. The surface morphology of the deposits' materials has been investigated using AFM. Undoped ZnO, ZnO:1% Mn, and ZnO:3% Mn nanoparticles were found to have grains between 92.6, 85.7, and 47.8 nm in size, respectively. SEM images illustrate a significant transformation from flat islands to spherical nano-grains following Manganese doping in ZnO films. The transmittance in the visible range is greater than 78 %. The absorption coefficient decreased by increasing Mn content, and the optical bandgap values decreased from 3.32 to 3.21 eV with an increase in manganese-doped zinc oxide. The extraction coefficient and refractive index are lower with manganese concentration in zinc oxide thin films.Hydrogen gas reduces resistance in ZnO films, indicating p-type behavior. Doping with 3% Mn increases resistance. Decreasing sensitivity with higher Tin content in hydrogen gas exposure indicates elevated electrical resistance.

Acknowledgements

Mustansiriyah University (www. uomustansiriyah.edu.iq) and Alnukhba University College is supporting this project.

References

[1] A. Jilani, M.S. Abdel-wahab, H.Y. Zahran, I.S. Yahia, A.A. Al-Ghamdi, Appl. Phys. A., 122, 862–11(2016); https://doi.org/10.1007/s00339-016-9829-y

[2] R. Kumar, O. Al-Dossary, G. Kumar, A. Umar, Nano-Micro Lett., 7, 97–120 (2015);

https://doi.org/10.1007/s40820-015-0030-4

[3] Mendoza, M.A.R., Casanova, D., Oliva, A.I., ECS J. Solid State Sci. Technol., 9, 103002 (2020); https://doi.org/10.1149/2162-8777/abcc57

[4] R. Vittal, K.-C. Ho, Renew. Sustain. Energy Rev., 70, 920–935 (2017);
https://doi.org/10.1016/j.rser.2016.12.008

[6] F. A. Jasima , Z. S. A. Mosa, N. F. Habubi, Y. H. Kadhim, S. S. Chiad, Digest Journal of Nanomaterials and Biostructures, 18 (3), 1039–1049 (2023);
https://doi.org/10.15251/DJNB.2023.183.1039

[6] R. Kumar, G. Kumar, O. Al-Dossary and A. Umar, Mater. Express, 5, (1) (2015);
https://doi.org/10.1166/mex.2015.1154

[7] X.H. Wang, B. Yao, D.Z. Shen, Z.Z. Zhang, B.H. Li, Z.P. Wei, Y.M. Lu, D.X. Zhao, J.Y. Zhang, X.W. Fan, L.X. Guan, C.X. Cong, Solid State Commun., 141 600–604 (2007);
https://doi.org/10.1016/j.ssc.2006.12.015

[8] A. A. Abdul Razaq , F. H. Jasim , S. S. Chiad , F. A. Jasim, Z. S. A. Mosa , Y. H. Kadhimd, Journal of Ovonic Research, 20 (2), 131 – 141 (2024); https://doi.org/10.15251/JOR.2024.202.131

[9] K. J. Chen, F. Y. Hung, S. J. Chang and S. J. Young, Journal of Alloys and Compounds, 479 (1-2), 674-677 (2009); https://doi.org/10.1016/j.jallcom.2009.02.112

[10] A.S. Hassanien, A.A. Akl, A.H. Saaedi, Cryst.Eng.Comm., 20, 1716–1730 (2018);
https://doi.org/10.1039/C8CE00089A

[11] F. H. Jasim, H. R. Shakir, S. S. Chiad, N. F. Habubi, Y. H. Kadhi,, Jadan, M., Digest Journal of Nanomaterials and Biostructures, 18(4), 1385–1393 (2023);
https://doi.org/10.15251/DJNB.2023.184.1385

[12] Z. Liu, Z. Jin, W. Li, X. Liu, J. Sol-Gel Sci. Technol., 40, 25–30 (2006);
https://doi.org/10.1007/s10971-006-6990-1

[13] P.K. Shishodia, H.J. Kim, A. Wakahara, A. Yoshida, G. Shishodia, R.M. Mehra, J. Non. Cryst.Solids., 352, 2343–2346 (2006); https://doi.org/10.1016/j.jnoncrysol.2006.02.094

[14] Tang, P., Li, B., Feng, L, Ceram. Int., 44, 4154–4157 (2018);
https://doi.org/10.1016/j.ceramint.2017.12.170

[15] Al-Khawaja S, Abdallah B, Abou Shaker S, Kakhia M., Composite Interfaces., 22(3), 221-231(2015); https://doi.org/10.1080/09276440.2015.1075016

[16] A.A. Al-ghamdi, H. Alhumminay, M.S. Abdel-wahab, I.S. Yahia, Opt. Int. J. Light Electron Opt., 127, 4324–4328 (2016); https://doi.org/10.1016/j.ijleo.2016.01.110

[17] Qiu, J., Guo, B., Zhang, H., Yu, C., Li, F., J. Phys. Chem. C, 122, 24542–24549 (2018);
https://doi.org/10.1021/acs.jpcc.8b08626

[18] S.J. Lim, S. Kwon, H. Kim, Thin Solid Films, 516, 1523–1528 (2008);
https://doi.org/10.1016/j.tsf.2007.06.126

[19] R.S. Gaikwad, G.R. Patil, M.B. Shelar, B.N. Pawar, R.S. Mane, S.H. Han, O.S. Joo, Int. J. Self-Propagating High-Temperature Synth., 21, 178–182 (2012);
https://doi.org/10.3103/S1061386212030131

[20] Jeong, J.-K., Yun, H.-J., Yang, S.-D., Eom, K.-Y., Chea, S.-W., Park, J.-H., Lee, H.-D., Lee, G.-W., Thin Solid Films, 638, 89–95 (2017);
https://doi.org/10.1016/j.tsf.2017.07.043

[22] E. H. Hadi, D. A. Sabur, S. S. Chiad, N. F. Habubi, K., Abass, Journal of Green Engineering, 10 (10), 8390-8400 (2020); https://doi.org/10.1063/5.0095169

[23] K. S. Sharba, A. S. Alkelaby, M. D. Sakhil, K. H. Abass, N. F. Habubi, S. S. Chiad, Enhancement of urbach energy and dispersion parameters of polyvinyl alcohol with Kaolin additive, NeuroQuantology, 18 (3), 66-73 (2020);
https://doi.org/10.14704/NQ.2020.18.3.NQ20152

[24] M. D. Sakhil, Z. M. Shaban, K. S. Sharba, N. F. Habub, K. H. Abass, S. S. Chiad, A. S. Alkelaby, NeuroQuantology, 18 (5), 56-61 (2020);

https://doi.org/10.14704/nq.2020.18.5.NQ20168
[25] Khadayeir, A. A., Hassan, E. S., Mubarak, T. H., Chiad, S.S., Habubi, N. F., Dawood, M.O., Al-Baidhany, I. A., Journal of Physics: Conference Series, 1294 (2) 022009(2019); https://doi.1088/1742-6596/1294/2/022009
[26] N. Y. Ahmed, B. A. Bader, M. Y. Slewa, N. F. Habubi, S. S. Chiad, NeuroQuantology, 18(6), 55-60 (2020); https://doi.org/10.1016/j.jlumin.2021.118221
[27] A. J. Ghazai, O. M. Abdulmunem, K. Y. Qader, S. S. Chiad, N. F. Habubi, AIP Conference Proceedings 2213 (1), 020101 (2020); https://doi.org/10.1063/5.0000158
[28] H. A. Hussin, R. S. Al-Hasnawy, R. I. Jasim, N. F. Habubi, S. S. Chiad, Journal of Green Engineering, 10(9), 7018-7028 (2020); https://doi.org/10.1088/1742-6596/1999/1/012063
[29] S. S. Chiad, H. A. Noor, O. M. Abdulmunem, N. F. Habubi, M. Jadan, J. S. Addasi, Journal of Ovonic Research, 16 (1), 35-40 (2020). https://doi.org/10.15251/JOR.2020.161.35
[30] H. T. Salloom, E. H. Hadi, N. F. Habubi, S. S. Chiad, M. Jadan, J. S. Addasi, Digest Journal of Nanomaterials and Biostructures, 15 (4), 189-1195 (2020);
https://doi.org/10.15251/DJNB.2020.154.1189
[31] R. S Ali, N. A. H. Al Aaraji, E. H. Hadi, N. F. Habubi, S. S. Chiad, Journal of Nanostructuresthis link is disabled, 10(4), 810–816 (2020); https://doi: 10.22052/jns.2020.04.014
[32] A. A. Khadayeir, R. I. Jasim, S. H. Jumaah, N. F, Habubi, S. S. Chiad, Journal of Physics: Conference Series,1664 (1) (2020); https://doi.org/10.1088/1742-6596/1664/1/012009
[33] Sahoo, S.K., Mangal, S., Mishra, D., Kumar, P., Singh, U.P., Mater. Sci. Semicond. Process., 63, 76–82 (2017); https://doi.org/10.1016/j.mssp.2017.05.029
[34] N. N. Jandow, M. S. Othman, N. F.Habubi, S. S. Chiad, K. A. Mishjil, I. A. Al-Baidhany, Materials Research Express, 6 (11), (2020); https://doi.org/10.1088/2053-1591/ab4af8 [35] M. S. Othman, K. A. Mishjil, H. G. Rashid, S. S. Chiad, N. F. Habubi, I. A. Al-Baidhany, Journal of Materials Science: Materials in Electronics, 31(11), 9037-9043 (2020);
https://doi.org/10.1007/s10854-020-03437-0
[36] Kumar, K.D.A., Valanarasu, S., Rosario, S.R., Ganesh, V., Shkir, M., Sreelatha, C., Solid State Sci., 78, 58–68 (2018); https://doi.org/10.1016/j.solidstatesciences.2018.02.012
[37] E. S. Hassan, K. Y. Qader, E. H. Hadi, S. S. Chiad, N. F. Habubi, K. H. Abass, Nano Biomedicine and Engineering, 12(3), pp. 205-213 (2020);
https://doi.org/10.5101/nbe.v12i3.p205-213
[38] S. S Chiad,, A. S. Alkelaby, K. S. Sharba,, Journal of Global Pharma Technology, 11 (7), 662-665, (2020); https://doi.org/10.1021/acscatal.1c01666
[39] Chiad, S.S., Noor, H.A., Abdulmunem, O.M., Habubi, N.F., Journal of Physics: Conference Series 1362(1), 012115 (2019); https://doi.org/10.1088/1742-6596/1362/1/012115
[40] R. S. Ali, M. K. Mohammed, A. A. Khadayeir, Z. M. Abood, N. F. Habubi and S. S. Chiad, Journal of Physics: Conference Series, 1664 (1), 012016 (2020);
https://doi:10.1088/1742-6596/1664/1/012016
[41] A. S. Al Rawas, M. Y. Slewa, B. A. Bader, N. F. Habubi, S. S. Chiad, Journal of Green Engineering,10 (9), 7141-7153 (2020); https://doi.org/10.1021/acsami.1c00304
[42] R. S. Ali, H. S. Rasheed, N. F. Habubi, S.S. Chiad, Chalcogenide Letters,, 20 (1), 63–72 (2023; https://doi.org/10.15251/CL.2023.201.63
[43] B. A. Bader, S. K. Muhammad, A. M. Jabbar, K. H. Abass, S. S. Chiad, N. F. Habubi, J. Nanostruct, 10(4): 744-750, (2020); https://doi.org/ 10.22052/JNS.2020.04.007
[44] K. Y. Qader, R. A. Ghazi, A. M. Jabbar, K. H. Abass, S. S. Chiad, Reduce of energy gap of CuO Nano structure film by Ag doping, Journal of Green Engineering, 10 (10), 7387-7398 (2020); https://doi.org/10.1016/j.jece.2020.104011
[45] Y. Kang, F. Yu, L. Zhang, W. Wang, L. Chen, Y. Li, Solid State Ionics, vol. 360, p. 115544, 2021; https://doi.org/10.1016/j.ssi.2020.115544

[46] A. Ghazai, K. Qader, N. F. Hbubi, S. S. Chiad, O. Abdulmunem, IOP Conference Series: Materials Science and Engineering, 870 (1), 012027 (2020); https://doi.org/ 10.1088/1757-899X/870/1/012027
[47] O. M. Abdulmunem, A. M. Jabbar, S. K. Muhammad, M. O. Dawood, S. S. Chiad, N. F. Habubi, Journal of Physics: Conference Series,1660 (1), 012055 (2020); https://doi.org/ 10.1088/1742-6596/1660/1/012055
[48] E. H. Hadi, M. A. Abbsa, A. A. Khadayeir, Z. M. Abood, N. F. Habubi, and S.S. Chiad, Journal of Physics: Conference Series, 1664 (1), 012069 (2020); https://doi.org/ 10.1088/1742-6596/1664/1/012069
[49] K. Saritha, S. Rasool, K. R. Reddy, M. Tivanov, A. Saad, A. Trofimova, V. Gremenok, Mater. Res. Express 6, 106439 (2019); https://doi.org/10.1088/2053-1591/ab4078
[50] R. I. Jasim, E. H. Hadi, S. S. Chiad, N. F. Habubi, M. Jadan, J. S. Addasi, Journal of Ovonic Research, 19 (2), 187 – 196 (2023).
[58] H.T. Salloom, R. I. Jasim, N. F. Habubi, S. S. Chiad, M. Jadan, J. S. Addasi, Chinese Physics, 30 (6), 068505 (2021); https://doi.org/ 10.10.1088/1674-1056/abd2a7
[52 K. Y. Qader, E. H. Hadi, N. F. Habubi, S. S. Chiad, M. Jadan, J. S. Addasi, International Journal of Thin Films Science and Technology, 10 (1), 41-44 (2021); https://doi.org/ 10.18576/ijtfst/100107
[53] N. A. C. Lah, Surfaces and Interfaces, p. 102819, 2023; https://doi.org/10.1016/j.surfin.2023.102819